# On the pressure exerted by a bundle of independent living filaments

Jean-Paul Ryckaert\* and Sanoop Ramachandran Physique des Polymères, Université Libre de Bruxelles, Campus Plaine, CP 223, B-1050 Brussels, Belgium (Dated: August 18, 2018)

The properties of a bundle of grafted semi-flexible living filaments in ideal solution facing an obstacle wall, under supercritical conditions, are explored. For this purpose, we make use of the discrete wormlike chain model characterized by the monomer size d, a size dependent contour length  $L_{\rm c}$  and a persistence length  $l_{\rm p}$ . The calculation of the equilibrium filament size distribution and the average equilibrium force require the knowledge of the wall effect on the single filament partition function of any size, which can be computed by Metropolis Monte-Carlo methods. The force exerted by a living filament on a fixed wall turns out to be the weighted average of the dead grafted filament forces computed for sizes hitting the wall, multiplied by the probability of occurrence of the corresponding filament size. As the distance to the wall is varied, the resultant force shows large variations whose amplitude decrease with increasing gap sizes and/or with decreasing persistence length. Also, its average over a gap interval of precise size d gives an average force close to what is expected by the ratchet model for actin growth against a wall. The osmotic pressure exerted by  $N_f$  filaments is the average equilibrium force per filament times the grafting surface density.

## I. INTRODUCTION.

In eukaryotic cells, the various (de)polymerization reactions of cytoskeletal filaments such as actin and microtubules are coupled to various physical processes associated with cell motility. Some examples are the filopodia or lamellopodes whose underlying actin network structures grow against the cell membrane and hence develop protrusive forces and associated work. Similarly, the mobility of the pathogenic bacterium, lysteria, inside the infected cell results from a force originating from the build up of an actin network within a host cell at the rear of the bacterium membrane, which pushes forward the lysteria [1]. Focusing on the actin case in supercritical conditions, where the polymerization steps dominate, the direct or indirect measurement of these polymerizing forces for a controlled number of filaments have shown that they are of the order of a few pN per filament [2–5].

Statistical mechanics investigations on these polymerization forces require an explicit consideration of chemical reactions.

In his seminal papers [6, 7], T. L. Hill investigated the influence of tension or compression, within a straight polymerizing filament tethered at both ends, on the insertion probability of a monomer within the filament. If  $\rho_{1c}$  represents the monomer solution density in chemical equilibrium with monomers in the tension-free filament (zero internal force), he established that for an arbitrary monomer density  $\rho_1$ , the equilibrium will be attained when the filament internal force F (taken here as positive when compressive) reaches a value given by

$$F = \frac{k_{\rm B}T}{d}\ln\left(\frac{\rho_1}{\rho_{1c}}\right),\tag{1}$$

where d is the filament incremental contour length due to the insertion of a monomer in the structure. As an example, d is taken to be 2.7 nm for actin which is the half of the globular-actin (G-actin) diameter since filamentous-actin (F-actin) is a double stranded filament. For filaments with at least one free end, the equilibrium polymer model [1] establishes a critical concentration  $\rho_{1c}$  for which polymerization and depolymerization reactions proceed at equal rates at the actin filament end. In presence of a compressive force F, the mechanical energy of the (n+1)-mer exceeds the one of the n-mer by Fd. Hence the equilibrium constant is displaced towards depolymerization. Equation (1) is recovered via another interpretation of the critical density  $\rho_{1c}$  when F is the compressive force exerted at the tip of the filament which is needed to get chemical equilibrium at density  $\rho_1$ . Such a situation is relevant when a filament in supercritical conditions, grafted to an actin network at one side, is compressed by a membrane wall that its free ends encounters as it elongates. To interpret how actin monomers could intercalate in between the tip of the pushing filament and the wall (e.g. the bacterium membrane), Peskin et al. [8] suggested a Brownian ratchet model whereby the rigid filaments can grow against a wall subjected to an opposite load force by filling the sufficiently large gaps

<sup>\*</sup> jryckaer@ulb.ac.be

produced by the wall thermal fluctuations. This mechanism could not be validated as such experimentally, suggesting a close but alternative model, the elastic Brownian ratchet model whereby bending undulations of the filaments create the needed gap [9]. It must be stressed that it is generally believed that ultimate understanding for the force production in biological situations also requires a macroscopic viscoelastic treatment of the actin gel from which some individual filaments originate to transmit forces [10].

A relatively simple actin network is found at the tip of filopodial structures. A bundle of grafted filaments emerges from a network of cross linked parallel filaments and hits a membrane. Such a network has been the object of theoretical studies [11, 12] assuming a dynamical stochastic model for a set of parallel rigid living filaments pressing on a mobile rigid piston, always located at the level the longest filament of the bundle. The stalling force for a set of N non-interacting filaments is found to be N times the force per filament given by Eq. (1). In presence of lateral attractive interactions between filaments, the equilibrium force exerted by the bundle on the wall is enhanced by an additive contribution  $N \epsilon_l$ , where  $\epsilon_l$  is the attraction energy gain per unit length [12]. The stalling force needed to stop further polymerization of a network of parallel filaments in supercritical conditions was probed experimentally in vitro in [4] for a bundle of  $N_f \approx 10$  filaments, but the measured force was found to be considerably lower than  $N_f$  times the single filament force Eq.(1), an experimental result whose interpretation is still under debate [13, 14].

Seeking for a more microscopic description of a wall blocking a set of growing filaments, we have recently started a series of mesoscopic simulations of a bundle of grafted living biofilaments with persistence length  $l_p$ , in chemical equilibrium with explicit free monomers [15], based on the living filament model proposed earlier [16] in which intermolecular forces are explicitly taken into account. Each filament is modelled as a discrete chain of freely rotating stiff bonds, with a bending penalty term to adjust the persistence length. Its infinitely stiff bond limit corresponds to a discrete wormlike chain model characterized by three length scales, the contour length  $L_c$ , the persistence length  $l_p$  and the step length d corresponding to the contour length change per incorporated or leaving single monomer. Articulation points of the chain coinciding with Lennard-Jones centres of forces describe intermolecular interactions. In the simulated slit pore, the filaments anchored to one planar wall are growing in supercritical conditions and hit the opposing parallel wall located at a distance L from the first wall. An equilibrium situation is established when filament-wall forces become able to stop further growth of these filaments (in the average). These simulations are based on a formal Hamiltonian describing a set of  $N_1$  free monomers and a set of  $N_f$  filaments of varying size in contact with two parallel walls. While following the system composed of free monomers, grafted filaments and mesoscopic heat bath solvent particles by Molecular Dynamics, explicit Monte-Carlo moves do model the chemical (de)polymerizing steps in a way satisfying micro-reversibility [16]. In this way, our simulations sample a non-ideal reactive canonical ensemble for the grafted and confined bundle system. We find that the distribution of filaments lengths is exponential for sizes for which no direct interaction with the obstacle wall is possible. The wall presence induces the chemical species, corresponding to filaments with contour length longer than the gap size L, to bend and thus to store some effective compressional energy which more or less strongly, decreases their probability of occurrence at equilibrium. Hence, the size distribution decreases to zero over a few steps provided the supercriticality (chemical affinity) is appropriately limited to avoid lateral escape of very long filaments.

To interpret correctly the non-ideal effects related to monomer-monomer inter-filament interactions in the simulations, in particular the observed decrease of the pressure exerted by the filaments on the opposite wall [15], it is important to have a detailed understanding of the already complex ideal solution case where the filaments are independent. Such an ideal bundle system, in chemical equilibrium with free monomers, presents a rich set of properties which could not be developed in reference [15] and which is therefore the main theme covered by the present article. Two essential ingredients appear in the theoretical treatment. First, the free monomer reduced density  $\hat{\rho}_1 = K_0 \rho_1$ , where  $K_0$  is the (de)polymerizing equilibrium constant of a free-end in the ideal reference state imposes the degree of supercriticality (or possibly the degree of subcriticality) which is reflected by the characteristic length scale  $1/\ln \hat{\rho}_1$  associated to the exponential distribution of the short filament lengths. The tail of the distribution corresponding to long filament sizes requires wall factors  $\alpha_i(L; l_p, d)$ . These are related to single filament partition functions of a grafted filament of size i with fixed initial orientation, respectively in presence or in absence of the obstacle wall at a distance L from the seed grafting wall.

The paper is organized as follows. Section II provides the general thermodynamic description of the bundle of semi-flexible living filaments grafted at one wall, subject to single monomer (de)polymerization steps with free monomers of the bath, constrained within a slit pore with gap size  $L \ll l_{\rm p}$ . The specific statistical mechanics model of the filaments and the constraints or interactions imposed by the walls are formulated, allowing the derivation of the partition functions of the filaments of arbitrary size. And explicit account of the chemical reactions leads to the formal reactive canonical ensemble which provides the fundamental link with the Helmholtz free energy. Within the ideal bundle approximation, the distribution of filament sizes and the osmotic pressure or the osmotic force per filament are then derived from the explicit reactive ensemble partition function. The section ends with considerations on the limits of our theoretical approach, namely the existence of a maximum supercriticality  $\hat{\rho}_{1b}$  not to overcome to avoid any significant possibility for filaments to bend strongly over the gap distance L and start polymerizing parallel

to the obstacle wall.

In Section III, we transform the formal expressions for the wall factor into equivalent averages which turn out to be more appropriate for a single-filament/wall Monte-Carlo calculations, and we give details on their calculations for illustrative filament models, filament sizes and gap sizes. Most of the illustrations on the calculations of wall factors, filament size distributions at various reduced reduced free monomer densities and the corresponding equilibrium force for the living filaments, are concerned with the discrete wormlike chain model hitting a hard wall. We also provide an example with the finite stiffness version of our filament model hitting a specific continuous repulsive wall, using the model treated by our non-ideal simulations [15].

Section IV summarizes the outcomes of our study and concludes on some implications of our results.

#### II. THE CONFINED BUNDLE SYSTEM

# A. Statistical Mechanics description of the bundle of grafted living filaments

We are interested in a closed reacting ideal mixture at temperature T, having a fixed total number  $N_t$  of monomers which can either be free monomers (as a G-actin-ATP complex) or integrated within self-assembled filaments of variable length (as an actin-ATP complex in F-actin). This system is enclosed in a slit pore of volume V = AL with parallel walls of transverse area A and gap width L in which a fixed number  $N_f$  of independent filaments with variable contour length  $L_c$  and fixed persistence length  $l_p \gg L$  are grafted normal to one of the walls. The individual filaments of this bundle are continuously growing or shrinking through single monomers reversible (de)polymerization reactions at their free ends, consuming/rejecting free monomers in/from the bath so that, at each reacting event, the filament contour length jumps by a step length d representing the effective monomer size. This contour length  $L_c = (i-1)d$  is thus directly linked to the instantaneous total number of monomers i in the particular filament. In supercritical conditions where polymerization dominates, these semi-flexible filaments will grow and hit the obstacle formed by the opposite wall of the pore as soon as  $L_c > L$ . The global polymerization will be halted given the limited flexibility of the filaments and an equilibrium situation, characterized by an Helmholtz free energy  $F(T, A, L, N_t, N_f)$ , will be established for conditions we now establish.

The chemical reaction will be denoted as

$$A_{i-1} + A_1 \rightleftharpoons A_i \quad (3 < i \le z^*) \tag{2}$$

where  $A_i$  and  $A_1$  represent respectively an anchored filament of size i and a free monomer. This series of reactions is considered as limited to a size window going from a minimum filament size of three (to be considered as an effective permanent seed of the filament) up to a maximum size of

$$z^* = \frac{\pi L}{2d}. (3)$$

This upper limit corresponds to the size of a filament adopting a planar conformation of homogeneous curvature 1/L which, while satisfying end filament anchoring constraints and confinement, reorients its free end by 90 degrees and becomes able to further grow parallel to the wall surface without any further bending energy penalty. In the present work, we want to establish the compressive force originating from a bundle of relatively stiff filaments. We will restrict ourselves to thermodynamic conditions corresponding to a regime for which filaments of sizes approaching  $z^*$  are practically unpopulated because of their too high bending energy with respect to thermal fluctuations. These conditions are made explicit in the following paragraphs.

Starting with the general differential form of the free energy for a non-reacting mixture of  $N_1$  free monomers,  $N_3$  anchored filaments of three monomers,  $N_4$  anchored filaments of four monomers, ..., one would have

$$dF = -SdT - p_N AdL - p_T L dA + \mu_1 dN_1 + \sum_{i=3}^{z^*} \mu_i dN_i,$$
(4)

where the second and third reversible works terms imply the normal pressure  $(p_N)$  and tangential pressure  $(p_T)$  respectively. The other terms involve the chemical potentials  $\mu_1, \mu_3, \ldots$  of the different species. If we now relax the constraint of non-reactive mixture and impose the chemical equilibrium for all reactions in Eq. (2), we have

$$\mu_{i-1} + \mu_1 = \mu_i \quad (3 < i \le z^*). \tag{5}$$

At the same time, we impose that the relevant composition variables are  $N_t$  and  $N_f$ , related to species composition variables by

$$N_t = N_1 + 3N_3 + 4N_4 + 5N_5 + \dots + z^* N_{z^*}, \tag{6}$$

$$N_f = N_3 + N_4 + N_5 + \ldots + N_{z^*}. (7)$$

Taking into account Eqs. (5), (6) and (7), Eq. (4) becomes

$$dF = -SdT - p_N AdL - p_T L dA + \mu_1 dN_t + (\mu_3 - 3\mu_1) dN_f,$$
(8)

implying that the normal pressure  $p_N$  and the free monomer chemical potential  $\mu_1$  are given by

$$p_N = -\frac{1}{A} \left( \frac{\partial F}{\partial L} \right)_{N_t, N_f, A, T}, \tag{9}$$

$$\mu_1 = \left(\frac{\partial F}{\partial N_t}\right)_{N_f, A, L, T}.$$
(10)

The link with statistical physics is given by  $\beta F = -\ln Q^{\rm RC}$ , where the reactive canonical ensemble expression  $Q^{\rm RC}(N_t, N_f, L, A, T)$  relative to the anchored bundle system simplifies in the ideal solution approximation to [17]

$$Q^{\text{RC}} = \sum_{N_1, N_3, \dots} \frac{q_1^{N_1}}{N_1!} q_3^{N_3} \dots q_z^{N_z} \dots q_{z+k^*}^{N_{z+k^*}} \frac{N_f!}{N_3! \dots N_z! \dots N_{z+k^*}!}, \tag{11}$$

where the sum runs over all distinct possible arrangements of  $N_t$  monomers into various numbers of  $N_1$  free monomers,  $N_3$  filaments of length i=3,  $N_4$  filaments of length  $i=4,\ldots$  and  $N_{z+k^*}$  filaments of the largest size allowed  $z^*=z+k^*$ , which satisfy the two constraints, Eqs. (6) and (7). The factor  $q_1$  is the free monomer partition function while all  $q_i$  factors  $(3 \le i \le z^*)$  are partition functions of single anchored filaments of size i. We specify our model by choosing to describe our filaments as discrete wormlike chains with step length d and persistence length  $l_p$ , in contact with a hard wall when  $L_c > L$ . This can be expressed as

$$q_i(L) = \lim_{k \to \infty} \frac{1}{h^{3i}} \int dr^i \int dp^i \exp(-\beta H_i) \delta(x_1) \delta(y_1) \delta(z_1) \delta(x_2 - d) \delta(y_2) \delta(z_2), \tag{12}$$

where the  $\delta$  functions impose the normal grafting of the filament in the plane located at x=0 and where  $H_i$  is the Hamiltonian system of the filament of length i with intramolecular interactions including a stiff bond potential with a force constant k on which the limit is taken to fix the contour length.  $H_i$  also contains external interactions with the obstacle wall located at x=L but no other interactions with the grafting wall given the limited flexibility of the filaments. The explicit Hamiltonian  $H_i$  reads

$$H_{i}(\mathbf{r}, \mathbf{p}) = \sum_{j=1}^{i} \frac{\mathbf{p}_{j}^{2}}{2m} - (i - 1)\epsilon'_{0} + \sum_{j=1}^{i-1} \frac{k}{2} (d_{j} - d)^{2} + \frac{\kappa}{d} \sum_{j=2}^{N-1} (1 - \cos \theta_{j}) + \frac{i - 1}{2\beta} \ln \left[ \frac{2\pi}{\beta k d^{2}} \right] + U_{i}^{\text{ext}},$$
(13)

which starts with the kinetic energy term. The second term expresses the bonding energy corresponding to the energy released as heat when a new monomer attaches the filament and forms a new bond. There are i-1 bonds  $d_j = r_{j+1} - r_j$  of length d as we will consider in the third term stiff harmonic springs with  $d_j$  supposed to oscillate harmonically around d. The next term accounts for the bending energy where  $\theta_j$  is the bending angle between bonds  $d_{j-1}$  and  $d_j$ , while the bending modulus  $\kappa$  fixes the persistence length  $l_p$  of the filament according to  $\kappa = k_B T l_p$ . The constant fifth term is needed to normalize the exp  $\left[-\beta k(d_j-d)^2/2\right]$  term which will appear in the filament canonical partition function (or in any phase space integral) in order to allow the (scalar) Gaussian bond length distribution around the mean d to properly evolve towards the delta function in the  $k \to \infty$  limit. On this issue, it must be stressed that when taking the free filament Hamiltonian Eq.(13) without the external potential term, the integration of  $\exp(-\beta H)$  over all Cartesian momenta and over all bond length variables  $d_j$  followed by taking the infinitely stiff spring limit, leads to the usual discrete form of the wormlike chain effective configurational free energy

$$E_N[(\theta_j)_{j=2,(i-1)}] = -(i-1)\epsilon_0' + \frac{\kappa}{d} \sum_{j=2}^{i-1} (1 - \cos \theta_j).$$
(14)

The external potential term is specified by by a hard wall term  $U^{w}(L-x_{i})$  so that

$$U_i^{\text{ext}}(L) = \sum_{j=z+1}^i U^{\text{w}}(L - x_j),$$
 (15)

where the lower index of the sum in Eq.(15) refers to index z(L) representing the largest filament size which does not interact with the obstacle. For the discrete WLC model, this index is given by

$$z = 1 + I(L/d), \tag{16}$$

where I(x) denoted the integer part of a real value. For the finite stiffness filament model used in Molecular Dynamics type calculations [16] or/and when soft repulsive walls with maximum range  $R_c$  are used, one should take

$$z = 1 + I(L^{\text{eff}}/d), \tag{17}$$

where  $L^{\rm eff} = L - R_{\rm c} - (\beta k)^{-1/2} (L - R_{\rm c})/d$  in which the last term takes into account the bond fluctuations (of the order  $1/\sqrt{\beta k}$ ) for a filament of contour length  $\approx L - R_{\rm c}$ .

# B. Filament partition function and the reactive canonical ensemble partition function of the bundle

The ideal filaments bundle partition function given by Eq.(11) requires all single monomer  $q_1$  and single grafted filament  $q_i$  partition functions. The free monomers are restricted in the pore volume V = AL so that for the ideal solution,

$$q_1 = \frac{V}{\Lambda^3},\tag{18}$$

where the integration of the canonical partition function over momenta leads to the free monomer thermal de Broglie wavelength  $\Lambda = \sqrt{\beta h^2/2\pi m}$ .

If we denote as  $q_i^0$  the partition function of the same grafted filament system in absence of the obstacle wall, we can thus write

$$q_i = q_i^0 \quad (3 \le i \le z),$$

$$q_i \equiv \alpha_i(L)q_i^0 \quad (z < i \le z^*),$$

$$(19)$$

where the second relationship defines the wall factor  $\alpha_i(L)$ , which also depends on parameters  $l_p$ , d and T. It is defined formally as

$$\alpha_i(L) = \frac{q_i(L)}{q_i^0} = \langle \exp\left(-\beta U_i^{\text{ext}}\right) \rangle_{i0}, \tag{20}$$

where  $\langle ... \rangle_{i0}$  is a single filament canonical average with the Hamiltonian  $H_i$  given by Eq. (13) and explicit grafting constraints (see Eq. (12)) but with the  $U_i^{\text{ext}}$  term turned off.

The equilibrium constant  $K_i$  of the chemical reaction series in Eq. (2) in the ideal solution for grafted filaments with obstacle wall present, is given by [17]

$$K_{i} = \frac{q_{i}}{q_{i-1}q_{1}/V} = \frac{q_{i}}{q_{i-1}}\Lambda^{3} = \frac{\alpha_{i}}{\alpha_{i-1}}\frac{q_{i}^{0}}{q_{i-1}^{0}}\Lambda^{3} \equiv \frac{\alpha_{i}}{\alpha_{i-1}}K^{0},$$
(21)

where  $\alpha_i = 1$  for  $i \leq z$  and  $\alpha_i$  is given by Eq. (20) for i > z, and where we have considered that the equilibrium constant for the chemical reaction in absence of obstacle, denoted as  $K^0$ , is independent of i. For our grafted filament model with stiff bonds defined by the Hamiltonian in Eq. (13), the equilibrium constant  $K^0$  is indeed given by the i independent expression

$$K_0 = \frac{q_i^0}{q_{i-1}^0} \Lambda^3 = 2\pi \exp(\beta \epsilon_0') \frac{d^4}{l_p} \left[ 1 - \exp\left(-2\frac{l_p}{d}\right) \right] F(w_0), \tag{22}$$

where the last factor, involving  $w_0 = \sqrt{\beta k d^2}$ , is a correcting factor for bond flexibility with relative fluctuations  $\sigma_d/d = w_0^{-1}$ ,

$$F(w_0) = \left(\frac{w_0^2}{2\pi}\right)^{1/2} \int_0^\infty du \, \exp\left[-\frac{w_0^2}{2}(u-1)^2\right]$$
$$= \frac{\left[\frac{1+\text{erf}[w_0]}{2}(1+w_0^2) + \frac{w_0}{\sqrt{2\pi}}\exp\left(-\frac{w_0^2}{2}\right)\right]}{w_0^2}.$$
 (23)

As  $F(w_0)$  satisfies the property  $\lim_{k\to\infty} F(w_0) = 1$ , the equilibrium constant of the discrete WLC, hence the superscript dWLC, follows as

$$K_0^{\text{dWLC}} = 2\pi \exp(\beta \epsilon_0') \frac{d^4}{l_p} \left[ 1 - \exp(-2l_p/d) \right].$$
 (24)

Exploiting Eqs. (18), (19), (20) and (21), we finally rewrite all single filaments partitions as

$$q_i = q_3^0 \left(\frac{K^0}{\Lambda^3}\right)^{i-3} \quad (3 \le i \le z),$$
 (25)

$$q_i(L) = \alpha_i(L)q_3^0 \left(\frac{K^0}{\Lambda^3}\right)^{i-3} \quad (z < i \le z^*).$$
 (26)

Substituting in Eq. (11) the individual filament partition functions by Eqs. (25) and (26), leads to

$$Q^{\text{RC}} = N_f! \ q_3^{N_f} \left(\frac{K^0}{\Lambda^3}\right)^{(N_t - 3N_f)} \times \sum_{N_1, N_2, \dots} \frac{\alpha_{z+1}^{N_{z+1}} ... \alpha_{z+k}^{N_{z+k}} ... \alpha_{z+k^*}^{N_{z+k^*}}}{N_1! N_3! ... N_z! N_{z+1}! ... N_{z+k}! ...} \left(\frac{K^0}{V}\right)^{-N_1}.$$
(27)

### C. Filament size distribution

The average number densities of free monomers and filaments in the thermodynamic limit can be estimated by searching for the largest term (constrained extremum) of the partition function  $Q^{RC}$  in Eq. (27), proceeding exactly like in the case of free filaments [16, 17]. This requires solving the constrained global minimum

$$\frac{\partial}{\partial N_1} \ln \left[ \frac{1}{N_1!} \left( \frac{K^0}{V} \right)^{-N_1} \right] - \lambda = 0, \tag{28a}$$

$$\frac{\partial}{\partial N_i} \ln \left[ \frac{1}{N_i!} \right] - i\lambda - \mu = 0 \qquad (i = 3, z), \tag{28b}$$

$$\frac{\partial}{\partial N_{z+k}} \ln \left[ \frac{\alpha_k^{N_{z+k}}}{N_{z+k}!} \right] - (z+k)\lambda - \mu = 0 \qquad (k=1,k^*), \tag{28c}$$

where  $\lambda$  and  $\mu$  are Lagrange multipliers related respectively to the constraints given by Eqs. (6) and (7). Use of the Stirling's approximation leads to the set of equations

$$\ln N_1 + \ln \left(\frac{K^0}{V}\right) + \lambda = 0, \tag{29}$$

$$ln Ni + i\lambda - \mu = 0 \qquad (i = 3, z), \tag{30}$$

$$\ln(N_{z+k}/\alpha_{z+k}) + (z+k)\lambda - \mu = 0 \qquad (k=1, k^*).$$
(31)

In terms of the free monomer reduced number density  $\hat{\rho}_1 = \rho_1 K^0$ , one gets

$$\hat{\rho}_1 = \exp\left(-\lambda\right),\tag{32}$$

$$N_i = \exp(-[i\lambda + \mu]) = \hat{\rho}_1^i \exp(-\mu) \qquad (i = 3, z),$$
 (33)

$$N_{z+k} = \alpha_{z+k} \exp\left(-\left[(z+k)\lambda + \mu\right]\right),\,$$

$$= \alpha_k \hat{\rho}_1^{z+k} \exp\left(-\mu\right) \qquad (k=1, k^*). \tag{34}$$

The combination of Eqs. (7), (33) and (34) gives  $\exp(-\mu) = N_f/D$  where D and filament densities are finally given (with L dependence made explicit) by

$$P_i(\hat{\rho}_1, L) = \frac{N_i}{N_f} = \frac{(\hat{\rho}_1)^i}{D}$$
 (3 \le i \le z(L)),

$$P_{z+k}(\hat{\rho}_1, L) = \frac{N_{z+k}}{N_f} = \alpha_{z+k}(L) \frac{(\hat{\rho}_1)^{z+k}}{D} \qquad (1 \le k \le k^*), \tag{36}$$

$$D(\hat{\rho}_1, L) = \left[\sum_{i=3}^{z} (\hat{\rho}_1)^i\right] + \sum_{k=1}^{k^*} \alpha_{z+k}(L)(\hat{\rho}_1)^{z+k}, \tag{37}$$

where z is fixed by the condition Eqs. (16) or (17) and where  $z^*$  was fixed by Eq. (3). The reduced density  $\hat{\rho}_1$  is itself the solution of an implicit equation obtained by substituting the filament densities Eqs. (35) and (36) in the constraint relationship Eq. (6), giving

$$\rho_t = \rho_1 + \rho_f \langle i \rangle = \rho_1 + \rho_f \frac{M(\hat{\rho}_1, L)}{D(\hat{\rho}_1, L)}, \tag{38}$$

where  $\rho_t$ ,  $\rho_f$  are respectively the total monomer and filament number densities and where  $\langle i \rangle$  is the average length of the filaments in the bundle. In Eq. (38), D is given by Eq. (37) and M by

$$M(\hat{\rho}_1, L) = \sum_{i=3}^{z} i(\hat{\rho}_1)^i + \sum_{k=1}^{k^*} (z+k)\alpha_{z+k}(L)(\hat{\rho}_1)^{z+k} \equiv \hat{\rho}_1 \frac{\partial D}{\partial \hat{\rho}_1}.$$
 (39)

### D. Bundle pressure and individual filament force exerted on the opposite wall

Equations (35), (36) and (38) provide the population densities, compatible with the constraints, which correspond to the largest term in the reactive canonical partition function  $Q^{\rm RC}$  (27) and which can be identified, in the thermodynamic limit, as the equilibrium densities  $\langle N_1 \rangle / V$  or  $\langle N_i \rangle / V$ . Restricting the partition function to its maximum term  $\tilde{Q}^{\rm RC}$ , we can now obtain the partial derivatives in Eqs. (9) and (10) from the Helmholtz free energy

$$-\beta F = \ln \tilde{Q}^{\text{RC}} = C(N_f, T) + N_t \ln \left(\frac{K_0}{\Lambda^3}\right) + \sum_{k=1}^{k^*} \langle N_{z+k} \rangle \ln \alpha_{z+k}$$
$$+ N_1 - N_1 \ln \left(\langle N_1 \rangle K_0 / V\right) - \sum_{i=3}^{z^*} \langle N_i \rangle \ln \langle N_i \rangle + N_f, \tag{40}$$

where  $C(N_f,T) = \ln \left[ N_f! (K_0/\Lambda^3)^{-3N_f} q_3^{N_f} \right]$ , using chemical densities provided by Eqs.(35), (36) and (38). Substituting for the number of filaments at equilibrium, one gets

$$-\beta F = C(N_f, T) + N_t \ln\left(\frac{K_0}{\Lambda^3}\right) + N_1 - N_1 \ln \hat{\rho}_1$$
$$-N_f \langle i \rangle \ln \hat{\rho}_1 + N_f - N_f \ln N_f + N_f \ln D. \tag{41}$$

Using the conservation of the total number of monomers  $N_t = N_1 + N_f \langle i \rangle$ , see Eq. (38), the free energy Eq. (41) can be simplified and expressed in terms of independent variables and in terms of the intermediate  $\hat{\rho}_1$ , given the lack of an explicit  $\hat{\rho}_1(N_t, N_f, A, L, T)$  dependency,

$$\beta F = C'(N_f, T) - \frac{AL}{K_0(T)} \hat{\rho}_1 + N_t \ln\left(\frac{\hat{\rho}_1 \Lambda^3(T)}{K_0(T)}\right) - N_f \ln D(\hat{\rho}_1, L), \tag{42}$$

where we have introduced  $C' = -C - N_f + N_f \ln N_f$ .

We first check the consistency of the final free energy expression by combining Eqs. (10) and (42) to get the ideal solution expression of the chemical potential  $\mu_1$ ,

$$\beta \mu_1 = \left(\frac{\partial(\beta F)}{\partial N_t}\right) + \left(\frac{\partial(\beta F)}{\partial \hat{\rho}_1}\right) \left(\frac{\partial \hat{\rho}_1}{\partial N_t}\right),\tag{43}$$

$$= \ln\left(\rho_1 \Lambda^3\right) - \left(\frac{AL}{K_0} - \frac{N_t}{\hat{\rho}_1} + \frac{N_f \langle i \rangle}{\hat{\rho}_1}\right) \left(\frac{\partial \hat{\rho}_1}{\partial N_t}\right),\tag{44}$$

$$= \ln\left(\rho_1 \Lambda^3\right),\tag{45}$$

where the expected result for an ideal solution follows by successively exploiting Eqs. (39) and (38).

Combining similarly Eqs. (9) and (42) , we get the pressure  $p_N$ 

$$\beta p_N = -\left(\frac{\partial(\beta F/A)}{\partial L}\right) - \left(\frac{\partial(\beta F/A)}{\partial \hat{\rho}_1}\right) \left(\frac{\partial \hat{\rho}_1}{\partial L}\right),\tag{46}$$

$$= \rho_1 + \sigma_f \left(\frac{\partial \ln D}{\partial L}\right)_{\hat{\rho}_1},\tag{47}$$

where  $\sigma_f = N_f/A$  is the filament surface density. Isolating the osmotic pressure  $\Pi = p - p^*$  where  $p^* = \rho_1 k_B T$ , one finally gets the osmotic normal force per filament  $f_N(L, \hat{\rho}_1)$  in an ideal solution as

$$\beta f_N = \frac{\pi}{\sigma_f k_{\rm B} T} = \left(\frac{\partial \ln D}{\partial L}\right),$$

$$= \frac{\sum_{k=1}^{k^*} \frac{\partial \alpha_{z+k}(L)}{\partial L} (\hat{\rho}_1)^{z+k}}{D} = \sum_{k=1}^{k^*} \frac{\partial \ln \alpha_{z+k}(L)}{\partial L} P_{z+k}(\hat{\rho}_1, L),$$
(48)

$$= \sum_{k=1}^{k^*} \beta \mathbf{f}_{z+k}(L) P_{z+k}(\hat{\rho}_1, L), \tag{49}$$

where we have introduced a fixed length filament mean force and associated mean force potential

$$\mathbf{f}_{z+k}(L) = -\frac{\partial W_{z+k}(L)}{\partial L},\tag{50}$$

$$W_{z+k}(L) = -k_{\rm B}T \ln \alpha_{z+k}(L). \tag{51}$$

Equation (49) gives the equilibrium force exerted on a living grafted filament by a fixed planar wall located at a distance L from the wall to which the filament is grafted. As expected, it is a weighted average of the force exerted by the wall on a fixed length grafted filament (an average over its internal degrees of freedom) where each filament size has an absolute probability  $P_{z+k}(\hat{\rho}_1, L)$ . Of course, only the filaments longer than z contribute.

### E. Chemical thermodynamic conditions for the applicability of the above theory

Apart for the ideal solution conditions which allow us to treat a chemical equilibrium of otherwise independent entities, we insisted from the beginning about the necessary condition  $P_{z^*} \cong 0$ , where  $z^*$  is given by Eq. (3). Indeed, especially in supercritical conditions where filaments tend to grow continuously, the filaments must be sufficiently rigid to resist a bending turn of 90 degrees with respect to their initial orientation at grafting, normal to the wall. One should avoid that, by exploiting a rare but possible bending thermal fluctuation, the filament could find the way to continue its polymerization along the obstacle wall with no further bending energy penalty. This can be imposed by requesting that

$$\frac{P_{z^*}(L,\hat{\rho_1})}{P_z(\hat{\rho_1})} = \alpha_{z^*}(L)\hat{\rho_1}^{(z^*-z)} \ll 1, \tag{52}$$

which implies, using for the force at any compression  $(L_{ci} - L)$ , the buckling force expression for a filament of size i and contour length  $L_{ci}$ , namely [18]  $\beta f_{bi} = (\pi^2/4)(l_p/L_{ci}^2)$ , the inequalities

$$-\beta W_{z^*}(L) + (z^* - z) \ln \hat{\rho}_1 < 0,$$
  
$$-\beta f_{bz^*}(\frac{\pi}{2} - 1)L + (\frac{\pi}{2} - 1)\frac{L}{d} \ln \hat{\rho}_1 < 0,$$
 (53)

and so finally, the condition on the reduced density

$$\ln \hat{\rho}_1 < \frac{l_p d}{L^2} \equiv \ln \hat{\rho}_{1b},\tag{54}$$

where  $\hat{\rho}_{1b}$  is the upper limit of the reduced free monomer density.

# III. MONTE-CARLO DETERMINATION OF THE WALL FACTORS AND ILLUSTRATIVE APPLICATIONS

# A. Monte-Carlo method

We consider a filament modelled by the Hamiltonian  $H_i$  given in Eq. (13) subject to grafting conditions at the wall in the plane at x=0 as formulated in Eq. (12). Eq. (15) provides the external potential due to the sum of individual interactions  $U^{\rm w}(L-x)$  between any monomer in the range of interaction  $(L-r_c < x < L)$  and the obstacle wall located at x=L. We consider generally a large but finite stretching force constant k but we will also be interested in the discrete WLC model obtained in the  $k \to \infty$  limit. The conditions Eqs. (16) and (17) define the portion of the filament which does not interact with the wall directly. The wall factor for a grafted filament of size i > z is given formally by Eq.(20) which can be rewritten as

$$\alpha_i(L) = \left\langle \exp\left(-\sum_{k=z+1}^i \beta U^{\mathbf{w}}(L - x_k)\right) \right\rangle_{i0}.$$
 (55)

Given the additivity of the various contributions to the Hamiltonian  $H_i$  of a grafted filament in absence of obstacle wall and given the various simplifications between similar integrals in the numerator and the denominator in the average Eq. (55), one can rewrite the average Eq. (55) over an ensemble associated to a single filament of size i as another average over a single filament of size i, in which the quantity to be averaged still contains an explicit integration of the remaining portion of the filament between i and i, which must still be performed for each microscopic configuration of the main filament portion of size i and i, which must still be performed for each successive local Cartesian coordinate systems for the extra bonds of index i and i

$$\alpha_i(L,T) = \left(\frac{1}{F(w_0)}\right)^{i-z} \left\langle \prod_{j=z}^{i-1} \int d\mathbf{W}_j \exp\left[-\beta U^w(L-x_{j+1})\right] \right\rangle_z, \tag{56}$$

where the average  $\langle \ldots \rangle_z$  indicates an average over the configuration space of a grafted filament of size z which does not interact with any wall, where  $x_{j+1}$  is the x coordinate of the monomer of index j+1 depending on the coordinates of the primary grafted chain of size z and of the additional sampled coordinates of the bonds  $z, z+1, \ldots, z+j-1$  of the extra piece of the filament.  $U^w(L-x)$  is the wall potential acting on a monomer located at x < L. Finally, the integration  $dW_j$  over the spherical coordinates  $t_j, \eta_j = \cos \theta_j, \phi_j$  is given by

$$\int d\mathbf{W}_{j} \equiv \int_{0}^{\infty} du_{j} \ u_{j}^{2} \int_{-1}^{+1} d\eta_{j} \int_{0}^{2\pi} d\phi_{j} P_{u}(u_{j}) P_{\eta}(\eta_{j}) P_{\phi}(\phi_{j}), \tag{57}$$

in terms, for any bond, of normalized distribution functions of u = t/d,  $\eta$  and  $\phi$ 

$$P_u = \frac{1}{\sqrt{2\pi(\beta k d^2)^{-1}}} \exp\left(-\frac{(u-1)^2}{2(\beta k d^2)^{-1}}\right),\tag{58}$$

$$P_{\eta} = \frac{\exp\left(-l_{\rm p}(1-\eta)/d\right)}{(d/l_{\rm p})[1-\exp\left(-2l_{\rm p}/d\right)]},\tag{59}$$

$$P_{\phi} = \frac{1}{2\pi}.\tag{60}$$

Note that this writing (with  $P_u$  improperly normalized as a Gaussian distribution which would sample u in the  $[-\infty, +\infty]$  range), it is possible to replace  $P_u$  by the  $\delta(u-1)$  function as  $k \to \infty$ .

Alternatively, using  $P'_u$  properly normalized on the  $[0, +\infty]$  range, we get

$$\alpha_i(L,T) = \left(\frac{V(w_0)}{F(w_0)}\right)^{i-z} \left\langle \prod_{j=z}^{i-1} \int d\mathbf{W}_j' \exp\left[-\beta U^w(L - x_{j+1})\right] \right\rangle_z, \tag{61}$$

where

$$\int d\mathbf{W}_{j}' \equiv \int_{0}^{\infty} du_{j} u_{j}^{2} \int_{-1}^{+1} d\eta_{j} \int_{0}^{2\pi} d\phi_{j} P_{u}'(u_{j}) P_{\eta}(\eta_{j}) P_{\phi}(\phi_{j}), \tag{62}$$

with

$$V(w_0) = \frac{\int_0^\infty \exp\left(-\frac{(u-1)^2}{2\sigma_d^2}\right)}{\int_{-\infty}^\infty \exp\left(-\frac{(u-1)^2}{2\sigma_d^2}\right)} = \frac{1 + \operatorname{erf}[w_0]}{2},\tag{63}$$

$$P'_{u} = \frac{\exp\left(-\frac{(u-1)^{2}}{2\sigma_{d}^{2}}\right)}{\int_{0}^{\infty} \exp\left(-\frac{(u-1)^{2}}{2\sigma_{d}^{2}}\right)} = P_{u}/V(w_{0}).$$
(64)

The wall factor  $\alpha_i$  in Eq. (61) can be computed as any average  $\langle \ldots \rangle_z$  by using a standard Metropolis Monte-Carlo sampling the configuration variables of a grafted filament of size z. For each microscopic configuration of the primary filament, a simple Monte-Carlo procedure is used to sample the  $3^{i-z}$  additional variables  $(u_j, \eta_j, \phi_j)$  in distributions  $P'_u$ ,  $P_\eta$  and  $P_\phi$  and hence solve numerically the multiple integral, what can be formulated

$$\alpha_{i}(L) = \left(\frac{V(w_{0})}{F(w_{0})}\right)^{i-z} \left\langle \lim_{M \to \infty} \frac{1}{M} \sum_{m=1}^{M} \left[ \prod_{j=z}^{i-1} \left( u_{jm}^{2} \exp\left[-\beta U^{w}\left((x_{j+1})_{m} - L\right)\right] \right) \right] \right\rangle_{z}, \tag{65}$$

where index m denotes a particular sampling of 3(i-z) variables, where  $(x_{j+1})_m$  is the x coordinate of monomer j+1, a function of the primary filament configuration variables and also function of all variables obtained in the  $m^{\text{th}}$  sampling for all intermediate bonds  $z, \ldots, z+j-1$ .

In the specific case of a infinitely stiff discrete WLC interacting with a hard wall for which  $\exp(-\beta U^{w}(L-x)) = \Theta(L-x)$  where  $\Theta(y)$  is the Heaviside function, Eq. (65) simplifies to

$$\alpha_i(L) = \lim_{M \to \infty} \left\langle \frac{1}{M} \sum_{m=1}^M \prod_{j=2}^{i-1} (\Theta(L - (x_{j+1})_m)) \right\rangle_{\mathcal{I}}.$$
 (66)

Use of Eqs. (65) and (66) require the sampling of i-z additional bond variables in distributions Eqs. (59) and (60). Each pair of  $\eta$ ,  $\phi$  variables can be obtained from two random numbers  $\xi_1$  and  $\xi_2$  sampled in a uniform distribution [0, 1] according to

$$\eta = 1 + \frac{d}{l_{\rm p}} \ln \left[ \xi_1 + (1 - \xi_1) \exp\left(-\frac{2l_{\rm p}}{d}\right) \right],$$
(67)

$$\phi = 2\pi \xi_2. \tag{68}$$

For sampling the u variable in Eq. (64) for flexible bonds appearing in Eq. (65), one samples a random number  $\xi_3$  in a normal Gaussian distribution with zero mean and the reduced bond length follows as

$$u = \xi_3 \frac{\sigma_d}{d} + 1 = \xi_3(w_0)^{-1} + 1. \tag{69}$$

If  $u \ge 0$ , u is accepted as a sampled reduced bond length while a value u < 0 is simply rejected and a new  $\xi_3$  sampling is performed (until a positive u value is obtained).

To conclude this section, let us point out that the determination of wall factors by Monte-Carlo can be performed in various other ways. The above procedure was found to be rather efficient as, using a single MC Metropolis sampling for any given z size primary filament, the  $\alpha_{z+k}(L)$  can be simultaneously estimated for  $k=1, k_{\text{max}}$  where  $k_{\text{max}} \cong 5$  and for L positions in the range going from  $L_{\text{min}} = (z-1)d$  up to a  $L_{\text{max}} = zd$ . We systematically performed four similar but independent runs (each of  $2 \times 10^6$   $(z-2)^2$  attempted steps) to use the dispersion of results to estimate the statistical errors. For the wall position variable, we used a discretization step  $\Delta L = 0.01d$  in order to estimate numerically the derivatives  $\partial \alpha/\partial L$  required to estimate the fixed length filament wall forces, Eqs.(50) and (51).

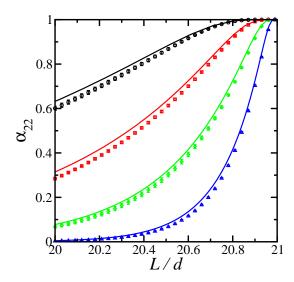


FIG. 1. The dependence of the wall-factor  $\alpha_{22}(L)$  on position of the wall for the discrete WLC model, for four different  $l_{\rm p}/d$  values, namely 1000 (blue triangles), 500 (green lozenges), 250 (red squares) and 125 (black circles). Statistical errors on  $\alpha_{22}$  data are indicated by  $\pm 1\sigma$  error bars. The continuous curves are plots of the unique universal curve for a similarly grafted continuous WLC hitting a hard wall [18], namely  $\alpha_{22}(L,l_{\rm p})=\tilde{Z}(\tilde{\eta})$ . Here, the definition of the scaling variable given by Eq. (70) is exploited along with  $L_{\parallel}=3.5d, 1.8d, 0.88d, 0.44d$  for the four  $l_{\rm p}$ 's in ascending order. Note that this continuous WLC theoretical curve is valid for the three largest  $l_{\rm p}$ 's but is supposed to be only approximately valid for  $l_{\rm p}/d=125$  as the criterium for validity of the universal regime is that the stiffness parameter satisfies  $L_{\rm c}/l_{\rm p}<0.1$  [18].

### B. Illustrative results

### 1. The wall factors

In Figs. 1 and 2, we illustrate the behaviour of  $\alpha_i(L)$  defined by Eq. (20) for a grafted discrete WLC hitting a hard wall, exploiting MC simulations data obtained via Eq.(66). We first show the results for a filament of size i=21 studied at moderate filament absolute compression, for various values of the persistence length. In all cases, the function reaches unity when the wall position L reaches from below the contour length of the originally compressed wormlike chain filament, but in a way which gets steeper as  $l_{\rm p}$  increases. Our MC results can be compared to the scaling properties of the continuous WLC model for a grafted filament of contour length  $L_{\rm c}$  and persistence length  $l_{\rm p}$  hitting a hard wall located at L [18]. The compression variable must be rescaled by a length  $L_{\parallel}$ , according to

$$\tilde{\eta} = \frac{(L_{\rm c} - L)}{L_{\parallel}},\tag{70}$$

$$L_{\parallel} = \frac{L_c^2}{l_{\rm p}}.\tag{71}$$

Adapting the general theoretical law to the specific cases shown in Figs. 1 and 2, we get close but distinct results with respect to our MC data dealing with a discrete chain. The MC results show systematically (also for other cases explored but not shown here) that the discrete chain (with respect to the continuous filament) requires more energy to be compressed by a similar absolute amount  $L_c - L$ . In Fig. 2, the behaviour of the wall coefficient  $\alpha_{21}(L)$  is shown overs a large L window which was obtained by assembling the results from four independent runs covering a different L window of size d. The comparison with the scaling law [18] shows again similarities and a somewhat stiffer behaviour of the discrete WLC (with step size d) with respect to its continuous limit, for identical  $l_p$ ,  $L_c$  and L parameters values.

### 2. Distributions of living filament sizes

Filament size distributions given in Eqs. (35), (36) and (37) are illustrated in Figs. 3 and 4 for a living, grafted (discrete) WLC hitting a hard wall, when exploiting the Monte-Carlo determined first five wall factors  $\alpha_{z+k}(L)$  beyond

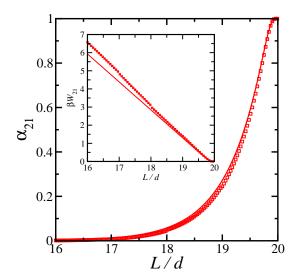


FIG. 2. The dependence of the wall factor  $\alpha_{21}(L)$  of a discrete WLC with persistence length  $l_{\rm p}/d=250$  over a range of wall positions L in the range L/d=16-20. The Monte-Carlo data are shown by symbols (note that statistical error bars on  $\alpha_{21}$  are smaller than the size of the symbols) while the continuous curve reproduces the universal curve  $\alpha_{21}(L,l_{\rm p})=\tilde{Z}(\tilde{\eta})$  [18], where the scaling variable  $\tilde{\eta}$  is given by Eq. (70) with  $L_{\parallel}=1.6d$ . In inset, the corresponding potential of mean force  $\beta W_{21}=-\ln\alpha_{21}$  is again compared (symbols for MC data) to the continuous WLC universal curve  $\beta \tilde{F}_{\parallel}(\tilde{\eta})$  [18], adapted to the present case.

the index z fixed by the gap size L/d (cfr Figs.1 and 2). In Fig. 3, the gap size L/d = 20 and hence the z = 21 value are fixed and the distributions are compared for various  $l_p$ 's while in Fig. 4, the distributions are shown for various gap sizes L/d, for a fixed persistence length  $l_p/d = 500$ . At the subcritical monomer density, one recognises in Fig.

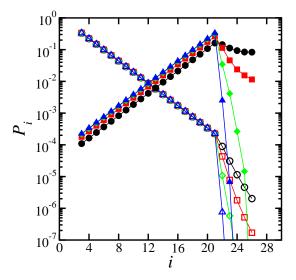


FIG. 3. Distributions of discrete WLC filament sizes, normalized in the  $i = [3, z + k_{max}]$  window  $(k_{max} = 5)$ , for a bundle of living filaments grafted at the left wall and confined by a hard obstacle wall with gap size L = 20d at subcritical  $\hat{\rho}_1 = 0.67$  (open symbols) and at supercritical  $\hat{\rho}_1 = 1.5$  (filled symbols) conditions for four different  $l_p/d$  values, namely 1000 (blue triangles), 500 (green lozenges), 250 (red squares) and 125 (black circles).

3 an exponential decay of short filaments densities followed by an even faster decay for the rare length fluctuations where filament sizes are able to hit the obstacle with their free ends. In the supercritical case, the wall interrupts the rising exponential distribution of short filaments densities but, for the same given pair of  $(L, \hat{\rho}_1)$  parameters, the  $l_p$  value, and hence the bending susceptibility, is seen to strongly influence the decay of the distribution beyond the size i = z. In Fig.(4), we fix the persistence length to  $l_p = 500d$  and fix the reduced free monomer density  $\hat{\rho}_1$  to a rather

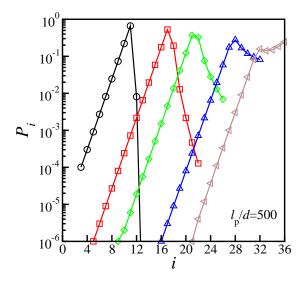


FIG. 4. Distributions of WLC filament sizes, normalized in the  $i = [3, z + k_{max}]$  window  $(k_{max} = 5)$ , for filaments with persistence length  $l_p/d = 500$  at  $\hat{\rho}_1 = 3.00$  for various gap widths L/d with associated z(L) index value, namely from left to right, L/d = 10.5 (circles), 16.5 (squares), 20.5 (lozenges), 26.5 (dark triangles) and 30.5 (light triangles).

large value and we compare the distributions for different hard wall gap sizes. We see that the convergence improves, as expected, when L gets smaller for fixed  $l_p$ ,  $\hat{\rho}_1$  values.

The convergence of the large filament size populations in supercritical conditions should always be controlled by the criterium provided in Eq. (54). Fast convergence towards zero for populations of filaments hitting the wall and in particular the requirement  $P(z^*) \cong 0$ , where  $z^*$  is defined by Eq. (3), requires  $\hat{\rho}_1 < \hat{\rho}_{1b} = \exp\left(l_{\rm p}d/L^2\right)$ . For data in Fig. 3 for which  $z^* = 31$  and  $\hat{\rho}_1 = 1.50$ , the inequality is verified for  $l_{\rm p}/d = 1000,500$  and 250 ( $\hat{\rho}_{1b} = 12.2,3.5$  and 1.9 respectively) but the criterium is not verified for  $l_{\rm p}/d = 125$  ( $\hat{\rho}_{1b} = 1.4$ ). This is coherent with the observed trends obtained numerically for the different  $l_{\rm p}$ 's for filaments sizes i = 22 up to  $i = 26 < z^*$ , the lowest value of  $l_{\rm p}$  suggesting a finite minimum in the distribution of filament lengths around a size  $z + 1 < i < z^*$ . In Fig. 4 where all data refer to  $\hat{\rho}_1 = 3$ , the same criterium is marginally verified for the gap sizes L/d = 20.5 with  $\hat{\rho}_{1b} = 3.3$  but not for the next gap size of L/d = 26.5 ( $z^* = 42$ ) for which  $\hat{\rho}_{1b} = 2.0$ . The poor convergence towards zero observed for the two wider gap sizes is again in agreement with the observation that  $\hat{\rho}_1 > \hat{\rho}_{1b}$ .

# 3. Equilibrium force exerted by a living filament on a fixed wall

The normal force Eq. (49) for a grafted filament hitting a wall can be computed for any value of the reduced free monomer density  $\hat{\rho}_1 < \hat{\rho}_{1b}$  provided the relevant series of wall factors  $\alpha_{z+k}(L)$  and their derivatives with respect to L are known. In Fig. 5, we report some results for the discrete WLC model. The variations of the equilibrium force with the gap size L over length scales below the monomer size d are seen to be enhanced as the persistence length increases. The origin of these variations can be easily interpreted for rather stiff living filaments. It is known [18] that the compressive force on a grafted filament of fixed length i increases from zero at L=(i-1)d towards the limiting buckling force  $f_c=(\pi^2/4)(k_{\rm B}T/L_{\parallel})$  where  $L_{\parallel}$  is given by Eq. (71), when the rescaled compression  $\tilde{\eta}$  defined by Eq.(70) is  $\approx 0.4$ . The behaviour of the equilibrium force in the range  $L/d=20 \rightarrow 21$  for  $l_{\rm p}/d=1000$  is essentially due to the action of filaments of length i=22 having a characteristic compression length  $L_{\parallel}=21^2/1000=0.44$ . Indeed there are no force contribution from shorter filaments and the probability to have longer filaments is marginal as it requires an absolute compression larger than d, hence a reversible work  $\approx df_c/(k_{\rm B}T) > 5$ . The observed increase of  $f_N(L)$  with L simply reflects the monotonic growth of the  $P_{22}(L)$  probability over the whole interval which is multiplied by a constant  $f_c$  until  $(21-L/d)\approx 0.4L_{\parallel}\approx 0.2$  where the force starts to decrease to zero as L/d further increases to 21.

Comparing forces for the same  $l_p$  and different reduced free monomer concentrations  $\hat{\rho}_1$ , we observe a systematic increase which can be quantified by the averaged force over the d interval. Using Eq. (48), the reduced averaged force turns out to be  $D(L+d,\hat{\rho}_1)/D(L,\hat{\rho}_1) \approx \ln \hat{\rho}_1$  as it can be qualitatively understood when noting that the wall factors appearing in  $D(L+d,\hat{\rho}_1)$  and  $D(L,\hat{\rho}_1)$  are in fact linked together by the approximate connection  $\alpha_i(L+d) \approx \alpha_{i-1}(L)$ . This result will be analyzed quantitatively and discussed in a biological context for the actin case in a separate

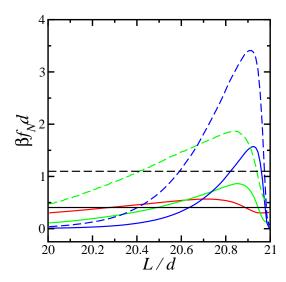


FIG. 5. For a right wall position between L/d=20 and L/d=21, evolution of the local reduced force  $\beta f_N d$  exerted by the right hard wall on one WLC filament starting at the left wall with first monomer at  $x=x_{wl}=0$ . The continuous (dashed) curves correspond to free monomer reduced number densities  $\hat{\rho}_1=1.5$  ( $\hat{\rho}_1=3.0$ ) and colours indicate  $l_p$  values ( $l_p/d=250$  (red),  $l_p/d=500$  (green),  $l_p/d=1000$  (blue)). The case  $l_p/d=250$ ,  $\hat{\rho}_1=3.0$  is not shown as  $\hat{\rho}_1>\hat{\rho}_{1b}$ . The black horizontal lines indicate levels of  $\ln \hat{\rho}_1$ , the continuous and dashed curves referring to  $\hat{\rho}_1=1.5$  and  $\hat{\rho}_1=3.0$  respectively.

publication [19].

We conclude these illustrations by the equilibrium force predicted for the grafted filament model that we used in direct simulations (using the Hybrid-Molecular Dynamics method) of a grafted bundle of interacting filaments, in chemical equilibrium with explicit free monomers, hitting the opposite wall [15]. The model (fully detailed in ref.[16]) is just a sum of single filament Hamiltonian terms given in Eq. (13) and free monomers Hamiltonian terms (point-mass particles) to which excluded volume intermolecular forces are added. Purely repulsive Weeks-Chandler-Andersen (WCA) interactions (with LJ parameters  $\sigma = 0.891d$  and  $\epsilon/k_{\rm B}T = 3$ ) operate between any pair of monomers belonging to different entities (entities are either free monomers or filaments). The monomer wall-interaction is taken as

$$U^{\mathbf{w}}(x) = \frac{3\sqrt{3}}{2} \epsilon_{\mathbf{w}} \left[ \left( \frac{\sigma_{\mathbf{w}}}{x} \right)^{9} - \left( \frac{\sigma_{\mathbf{w}}}{x} \right)^{3} \right] + \epsilon_{\mathbf{w}}$$
 (72)

where x is the wall-monomer distance, where  $\sigma_{\rm w}=d$  and  $\epsilon_{\rm w}/k_{\rm B}T=0.1$ . A cut-off is applied at potential minimum for  $x_c=1.200936d$ . In the simulations, the gap size was fixed to L/d=16 and the filament was modelled as follows: we adopt stiff bonds with a large but finite force constant  $k=400k_{\rm B}T/d^2$  giving rise to bond length fluctuations of the order  $\sigma_d/d=0.05$  and we chose a persistence length of  $l_{\rm p}=250d$  for the filaments.

We have computed using Eqs. (65) and (17) the first five wall factors  $\alpha_{16} - \alpha_{20}$  for the filament and the filament-wall interaction associated to the above MD model and looked at the equilibrium normal force  $f_N(L, \hat{\rho}_1)$  predicted in an ideal filament bundle solution where the present independent filament approach is relevant. The normal equilibrium force is shown in Fig. 6 in the range 15.5 < L/d < 16.5 for three values of  $\hat{\rho}_1$  below the limit  $\hat{\rho}_{1b} = 2.8$ . We observe again large variations and an average reduced force of the order of  $\ln \hat{\rho}_1$ .

### IV. CONCLUSIONS AND PERSPECTIVES

We have established the reactive canonical ensemble partition function corresponding to a set of independent living filaments undergoing (de)polymerizing reactions with free monomers from the bath, for a confined bundle system. Filaments are modelled as discrete wormlike chains grafted normally to one plane and confined by a second obstacle plane over a gap distance much shorter than the persistence length of the filaments. From this ideal system partition function, we have derived the distribution of filament sizes and the associated average force exerted by the living filaments on the opposite wall in supercritical conditions. We find strong oscillations of this equilibrium force with L varying, while any L averaged force over the single monomer size increment d turns out to be of the order of the expected result, Eq. (1). A more detailed analysis of the flexibility and the gap size influences of this averaged force will be discussed elsewhere [19]. We have also provided a Metropolis Monte-Carlo procedure to compute the

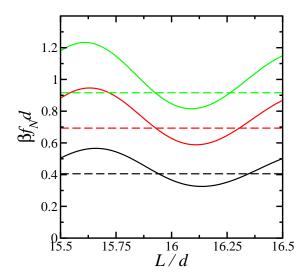


FIG. 6. Local reduced force  $\beta f_N d$  for a right wall position varying between L/d=15.5 and L/d=16.5. The three continuous curves (from bottom upwards) correspond to free monomer reduced number densities  $\hat{\rho}_1=1.5$ ,  $\hat{\rho}_1=2.0$  and  $\hat{\rho}_1=2.5$ . Horizontal lines of specific colour indicate levels of the corresponding  $\ln \hat{\rho}_1$  values, suggesting that the average force over the d interval is somewhat larger in the present case.

wall factors for various filaments/wall models. For the discrete wormlike chain hitting a hard wall, the results can be compared with the predictions of the continuous wormlike chain model for the same grafted filament/hard wall system [18]. The wall factors for the two models differ by a few percents, a result of the influence of the additional finite length scale d which seems to lead to a slightly less flexible model than the classical continuous WLC for an identical persistence length. This work on ideal bundles at equilibrium could be extended towards the analysis of the non equilibrium force-velocity relationship for a set of independent filaments pushing on a mobile piston against an external load. A possible route is to consider as stochastic variables the individual sizes of the different filaments and the one dimensional position of the piston using to describe the filament compression the potential of mean force  $W_i(L; l_p, d) = -k_B \ln \alpha_i(L; l_p, d)$  which takes into account the compression of the filaments. Work along these lines is in progress.

### ACKNOWLEDGMENTS

The authors wish to thank M. Baus, C. Pierleoni and G. Ciccotti for useful discussions about the present work. J.-P. R. hopes that the honoured and friend G. Ciccotti will appreciate the present work, despite the marginal use of Lagrange multipliers and the audacious choice of the infinitely stiff bond model for the discrete wormlike chain, avoiding the straight imposition of holonomic rigid bond constraints to enforce the filament fixed contour length property and therefore disregarding the beloved Jacobians! The authors warmly thank G. Destrée for invaluable technical help. S. Ramachandran acknowledges financial help from the BRIC Department (Bureau des Relations Internationales et de Coopération) of the Université Libre de Bruxelles.

<sup>[1]</sup> J. Howard, Mechanics of Motor Proteins and the Cytoskeleton (Sinauer, Sunderland, MA, 2001)

<sup>[2]</sup> D. Kovar and T. Pollard, Proc. Natl. Acad. Sci. USA 101, 14725 (2004)

<sup>[3]</sup> J. Berrot, A. Michelot, L. Blanchoin, D. Kovar, and J. Martiel, Biophys. J. 92, 2546 (2007)

<sup>[4]</sup> M. J. Footer, J. W. J. Kerssemakers, J. A. Theriot, and M. Dogterom, Proc. Natl. Acad. Sci. USA 104, 2181 (2007)

<sup>[5]</sup> C. Brangbour, O. du Roure, E. Helfer, D. Démoulin, A. Mazurier, M. Fermigier, M. Carlier, J. Bibette, and J. Baudry, PLoS Biol. 9, e1000613 (2011)

<sup>[6]</sup> T. L. Hill, Proc. Natl. Acad. Sci. USA 78, 5613 (1981)

<sup>[7]</sup> T. L. Hill and M. W. Kirschner, Proc. Natl. Acad. Sci. USA 79, 490 (1982)

<sup>[8]</sup> C. Peskin, G. Odel, and G. Oster, Biophys. J. 65, 316 (1993)

<sup>[9]</sup> A. Mogilner and G. Oster, Biophys. J. **71**, 3030 (1996)

- [10] R. Hawkins, M. Piel, G. Faure-Andre, A. Lennon-Dumenil, J. F. Joanny, J. Prost, and R. Voituriez, Phys. Rev. Lett. 102, 058103 (2009)
- [11] K. Tsekouras, D. Lacoste, K. Mallick, and J. Joanny, New J. Phys. 13, 103032 (2011)
- [12] J. Krawczyck and J. Kierfeld, EPL 93, 28006 (2011)
- [13] K. Tsekouras, D. Lacoste, K. Mallick, and J. Joanny, New J. Phys. 13, 103032 (2011)
- [14] A. Mogilner, J. Math. Biol. **58**, 105 (2009)
- [15] S. Ramachandran and J.-P.Ryckaert, J. Chem. Phys. **139**, 064902 (2013)
- [16] M. Caby, P. Hardas, S. Ramachandran, and J.-P.Ryckaert, J. Chem. Phys. 136, 114901 (2012)
- [17] T. L. Hill, An Introduction to Statistical Thermodynamics (Dover, New York, 1986)
- [18] A. Gholami, J. Wilhelm, and E. Frey, Phys. Rev. E 74, 041803 (2006)
- [19] work in progress(2013)